Thermodynamic Confinement and α-Helix Persistence Length in Poly(γ-benzyl-l-glutamate)-b-poly(dimethyl siloxane)-b-poly(γ-benzyl-l-glutamate) Triblock Copolymers

ARTICLE *in* BIOMACROMOLECULES · MARCH 2006

Impact Factor: 5.75 · DOI: 10.1021/bm050772t · Source: PubMed

6 AUTHORS, INCLUDING:

Periklis Papadopoulos
University of Ioannina
54 PUBLICATIONS **983** CITATIONS
SEE PROFILE

George Floudas
University of Ioannina
229 PUBLICATIONS **4,182** CITATIONS
SEE PROFILE

Thermodynamic Confinement and α-Helix Persistence Length in Poly(γ-benzyl-L-glutamate)-*b*-poly(dimethyl siloxane)-*b*-poly(γ-benzyl-L-glutamate) Triblock Copolymers

P. Papadopoulos and G. Floudas*

Department of Physics, University of Ioannina, P.O. Box 1186, 451 10 Ioannina, Greece, and Foundation for Research and Technology-Hellas, Biomedical Research Institute (FORTH-BRI)

I. Schnell and I. Lieberwirth

Max-Planck Institut für Polymerforschung, D-55021 Mainz, Germany

T. Q. Nguyen and H.-A. Klok

Laboratoire des Polymères, Institut des Matériaux, École Polytechnique Fédérale de Lausanne, CH-1015, Lausanne, Switzerland

Received October 16, 2005; Revised Manuscript Received December 1, 2005

The structure and the associated dynamics of a series of poly(γ-benzyl-L-glutamate)-*b*-poly(dimethyl siloxane)-*b*-poly(γ-benzyl-L-glutamate) (PBLG-*b*-PDMS-*b*-PBLG) triblock copolymers were investigated using small- and wide-angle X-ray scattering, NMR, transmission electron microscopy, and dielectric spectroscopy, respectively. The structural analysis revealed phase separation in the case of the longer blocks with defected α-helical segments embedded within the block copolymer nanodomains. The α-helical persistence length was found to depend on the degree of segregation; thermodynamic confinement and chain stretching results in the partial annihilation of helical defects.

I. Introduction

The advances in biotechnology in recent years have played a very important role in the development of new therapies. Peptides are always a vital part of the molecules designed for use in drug delivery or gene therapy, and thus, intensive studies on them have been carried out.[1] A great part of this work is focused on the control of the structure and dynamics of peptides and proteins, because both have an impact on their biological function. Changes in the secondary structure,[2] that is, the local conformation of the peptidic chain due to hydrogen bonding, can inhibit the action of these molecules, for example, as enzymes. In particular, the β-sheet secondary structure is known to be related to prion diseases.[3]

The study of the dynamics is also essential when one wants to understand protein folding and temperature- or solvent-induced changes in the structure, such as denaturation, or when specimen conservation is concerned. More specifically, the dynamic arrest known as the "glass transition" is known to inhibit the function of these molecules.[4,5] Some progress in this direction was made recently by studying the associated dynamics as a function of temperature, pressure, concentration, and peptide secondary structure.[6−8]

A step toward understanding the behavior of the large natural biological macromolecules is the study of peptide homopolymers or block copolymers. In the past, the difficulty of the synthesis of such molecules allowed only a limited number of such studies. Newly developed synthetic procedures can produce more complex and pure materials over a wide range of molecular weights.[9,10] However, this field is still unexplored to a great extent. Almost all previous studies report only on the static structure of these systems. An early example is a study by Gallot et al.[11] who investigated phase separation in diblock copolymers containing a peptide and a polyvinyl block. Other works include studies of diblock copolymers containing an α-helical peptide and an amorphous block, such as polystyrene-*b*-poly(γ-benzyl-L-glutamate) (PS-*b*-PBLG),[12] polyisoprene-*b*-(ε-carbobenzoxy-L-lysine) (PI-*b*-PZLys), and polyisoprene-*b*-poly(L-lysine) (PI-*b*-PLys).[13−17] In a more recent report, we investigated a series of PBLG oligopeptides, showing that the β-sheet structure is stable only at low degrees of polymerization and that the α-helix is favored at high molecular weights.[7] Furthermore, our study of a series of triblock copolymers containing PBLG and the water-soluble poly(ethylene oxide) (PBLG-*b*-PEO-*b*-PBLG) revealed that β-sheets can be destabilized by phase mixing but α-helices remain intact.[18] However, if PBLG is replaced by a different polypeptide such as poly(L-alanine), the β-sheet can be more stable, although again the peptidic chain consists mainly of α-helical parts.[19] Some works on similar systems containing alanine and leucine focused mainly on the biocompatibility of these materials.[20] A system that combines the two most important secondary structures (PBLG-*b*-polyglycine) revealed phase separation and dependence of the persistence lengths on composition.[21] It is noteworthy that phase separation was observed in almost all of the above systems, implying that peptides are highly incompatible with most synthetic macromolecules, probably because of unfavorable segment−segment interactions. Another important finding is that α-helices were found, in general, to be more stable than β-sheets, although deviations from the ideal structures are usual, such as folding or broken hydrogen bonds.

As we mentioned above, only an extremely limited number of works focus on the dynamics of such systems. Although dielectric spectroscopy (DS) measurements have been carried out in peptide solutions for a few decades,[22−27] the study of the

10.1021/bm050772t CCC: $33.50
Published on Web 01/07/2006

Table 1. Molecular Characteristics of the Four PBLG−PDMS−PBLG Copolymers

Sample PBLG-*b*-PDMS-*b*-PBLG	$\overline{M_{n,th}}$[a]	$\overline{M_n}$[b]	$\overline{M_w}$[b]	$\overline{M_w}/\overline{M_n}$[b]	$\overline{M_n}$[c]	f_{PBLG}[d]
5-24-5	3 966	3 280	3 990	1.22	3 966	0.49
50-271-50	41 954	38 200	48 600	1.27	55 094	0.57
50-24-50	23 676	34 500	47 500	1.38	32 436	0.93
100-24-100	45 576	44 650	54 270	1.22	60 030	0.96

[a] Calculated expected number-average copolymer molecular weight based on the molecular weight of the PDMS macroinitiator, as provided by the supplier, and the monomer−initiator ratio that was used. [b] Copolymer number-average molecular weight determined from GPC experiments carried out in DMF. [c] Copolymer number-average molecular weight determined from ^{1}H NMR spectra recorded in $CDCl_3$. [d] PBLG volume fraction: $f_{PBLG} = \upsilon_{PBLG}/(\upsilon_{PBLG} + \upsilon_{PDMS})$, where $\upsilon_{PBLG} = \overline{M_{n,PBLG}}/\rho_{PBLG}$ and $\upsilon_{PDMS} = \overline{M_{n,PDMS}}/\rho_{PDMS}$ ($\rho_{PBLG} = 1.278$ gcm^{-3}, $\rho_{PDMS} = 0.98$ gcm^{-3}, $\overline{M_n}$ from NMR).

dynamics in the bulk[28−32] is a relatively new field. DS is of particular importance, since it can follow the dynamics of the end-to-end dipole made within a rigid α-helical secondary structure. PBLG is one of the most thoroughly studied materials, and the first works in the bulk were reported by F. Kremer and other groups.[28−32] In recent DS studies[6−8] of PBLG oligopeptides as a function of molecular weight, temperature, pressure, and concentration, we showed that α-helices cannot be regarded as perfectly rigid; some hydrogen bonds are broken at "defected" places, and parts of the helix are allowed to relax independently. The large dipole along the peptidic backbone can be used as a probe of such "defects" that effectively reduce the dipole moment. In this sense, DS can be combined with "static" techniques to identify the particular perfection of peptide secondary structures.

Herein, we test the effect of thermodynamic confinement on the persistence length of PBLG helices by studying a series of PBLG-*b*-poly(dimethyl siloxane)-*b*-PBLG (PBLG-*b*-PDMS-*b*-PBLG) triblock copolymers. The synthesis of similar triblock copolymers was reported before, but no investigation of the structure and dynamics was made.[33,34] This system was chosen here because it combines PBLG with the very flexible PDMS that could result in higher incompatibility and stronger chain stretching. Indeed, all block copolymers but one with the lowest degree of polymerization exhibit nanophase separation. The different triblock copolymers have similar outer blocks (PBLG) but varying degrees of polymerization for the middle block (PDMS). The study on the dynamics revealed defected PBLG helices in the copolymers that could partially heal in the presence of a higher thermodynamic confinement, giving rise to chain stretching.

II. Experimental Section

Synthesis. Poly(γ-benzyl-l-glutamate)-*b*-poly(dimethylsiloxane)-*b*-poly(γ-benzyl-l-glutamate) (PBLG−PDMS−PBLG) triblock copolymers were prepared using commercially available α,ω-diamino poly(dimethylsiloxane)s as macroinitiator for the ring-opening polymerization of γ-benzyl-L-glutamate *N*-carboxyanhydride in THF as a solvent. Details of the monomer synthesis and the polymerization procedure have been reported earlier.[10,12] GPC traces of the crude product were multimodal and indicated the presence of PBLG homopolymer impurities, among others.

The crude PBLG-PDMS−PBLG triblock copolymers were purified using solid-phase extraction. For this purpose, 3-mL solid-phase extraction (SPE) cartridges ("Supelclean LC-NH2" from SUPELCO, Switzerland) were used. First, the cartridges were conditioned with 1 mL of distilled THF. After that, 1.5 mL of a solution containing 10 mg/mL of the crude polymer in THF was loaded on top of the cartridge. After equilibration, another 2 mL of distilled THF was added to the cartridge, and all the liquid which passed through was collected (fraction 1). In a second step, the cartridge was filled 3 times with 1 mL of a solution containing 95 vol % THF + 5 vol % DMF, and the eluted solution collected (fraction 2). Finally, 2 × 2 mL of an 80% THF + 20% DMF mixture was pushed through the cartridge (fraction 3). GPC analysis indicated that only fraction 2 contained the purified block copolymer. Excess THF was removed in a rotary evaporator, and the polymer was precipitated in methanol and isolated by centrifugation (3500 rpm, 5 min). After repeated washing with methanol, the solid was dried under vacuum at room temperature. Yield was about 30% of the initial weight of the crude material. The molecular characteristics of the final products are summarized in Table 1. The sample code gives the number-averaged degrees of polymerization for the triblock copolymers.

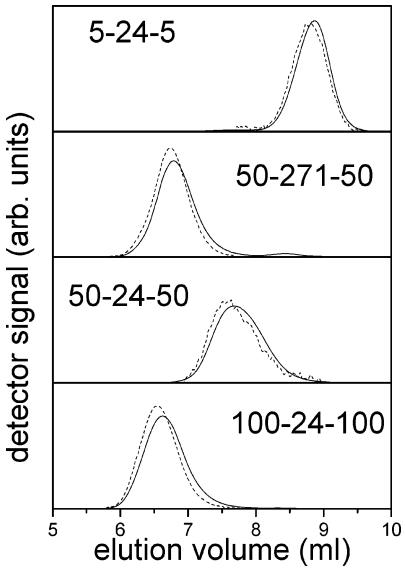

Figure 1. Gel permeation chromatography (GPC) curves of the four PBLG-*b*-PDMS-*b*-PBLG block copolymers investigated. The continuous and dashed lines correspond to the refractive index and the viscosity detector, respectively. The calculated molecular weights are shown in Table 1.

Gel Permeation Chromatography (GPC). Gel permeation chromatography (GPC) was performed on a Waters 150CV chromatograph modified for on-line differential viscometry. All analysis were carried out at 60 °C using a TSK-Gel Alpha 3000 column and DMF + 1 g/L LiBr as the eluent. Elution times were converted into absolute molecular weights using the "universal calibration" curve, which was constructed using anionically prepared poly(methyl methacrylate) standards, in combination with the information obtained from the refractive index and differential viscometer detectors. GPC traces of the four copolymers under investigation are shown in Figure 1.

^{13}C NMR. Solid-state ^{13}C cross-polarization magic-angle spinning (CPMAS) NMR spectra are shown in Figure 2 for five samples: $PBLG_{42}$ homopolymer, and $PBLG_{50}-PDMS_{271}-PBLG_{50}$, $PBLG_{50}-PDMS_{24}-PBLG_{50}$, $PBLG_{100}-PDMS_{24}-PBLG_{100}$, and $PBLG_5-PDMS_{24}-PBLG_5$ copolymers. The spectra were recorded on a Bruker spectrometer, operating at ^{1}H and ^{13}C Larmor frequencies of 700.13 and 176.05 MHz, respectively. A standard ^{1}H−^{13}C double-resonance fast-MAS probe was used, which supports rotors of 2.5 mm o.d. The samples

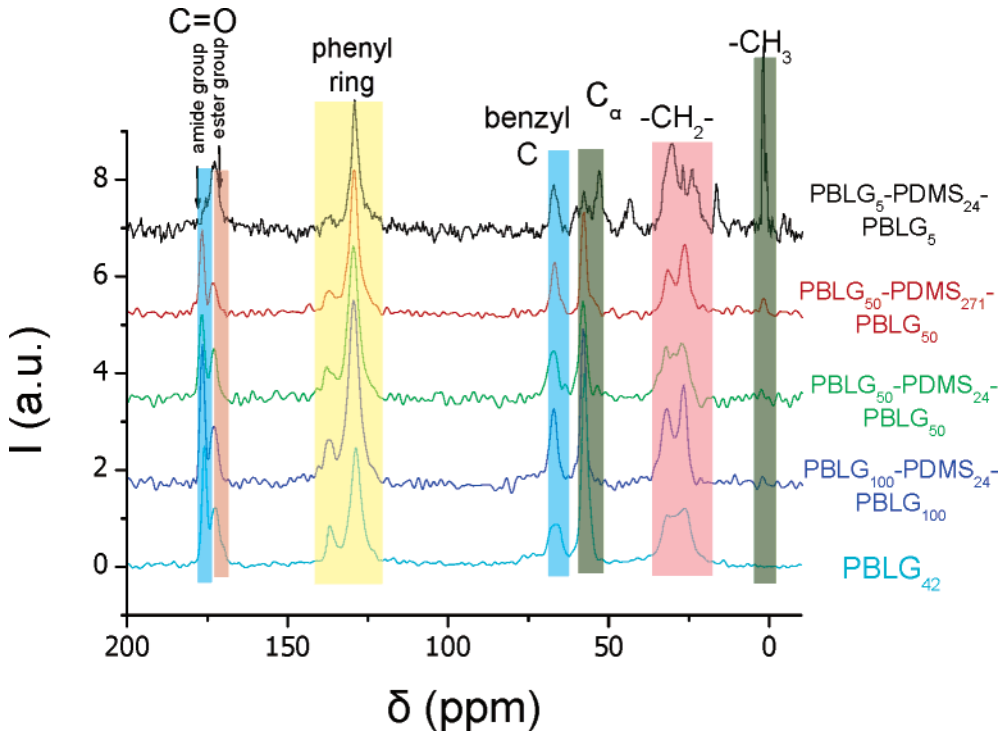

Figure 2. ^{13}C NMR spectra of a PBLG homopolymer and four block copolymers. (bottom to top): $PBLG_{42}$, $PBLG_5$-*b*-$PDMS_{24}$-*b*-$PBLG_5$ (f_{PBLG} = 0.49), $PBLG_{50}$-*b*-$PDMS_{271}$-*b*-$PBLG_{50}$ (f_{PBLG} = 0.57), $PBLG_{50}$-*b*-$PDMS_{24}$-*b*-$PBLG_{50}$ (f_{PBLG} = 0.93), $PBLG_{100}$-*b*-$PDMS_{24}$-*b*-$PBLG_{100}$ (f_{PBLG} = 0.96). In the $PBLG_5$-*b*-$PDMS_{24}$-*b*-$PBLG_5$, PBLG can be found in the β-sheet form, as indicated by the peak at $\delta \approx 53$ ppm corresponding to the α-carbon in the β-sheet conformation, whereas in all other cases, PBLG forms solely α-helices, as suggested by the C_α peaks at $\delta \approx 58$ ppm and the amide C═O resonances ($\delta \approx 177$ ppm).

were spun at 25 kHz MAS, which gives rise to an effective sample temperature of 310 K. A ramped CP contact pulse was applied for 1 ms, and the TPPM scheme was used for ^1H decoupling during ^{13}C signal acquisition. The signal was accumulated over 24k−48k transients of the CPMAS experiment.

X-ray Scattering. Both wide-angle and small-angle X-ray scattering (WAXS and SAXS) measurements have been performed. The WAXS measurements were made using a pinhole collimation and a two-dimensional (2D) detector (Siemens A102647) with 1024 × 1024 pixels. The Cu Kα radiation was used from a Siemens generator, and a graphite monochromator was used (λ = 0.154 nm). The sample-to-detector distance was 7.2 cm. Measurements were made from macroscopically oriented (extruded) filaments with a diameter of 0.7 mm, prepared at 353 and 373 K and followed by annealing at the same temperatures for 1 day. Subsequently, they were measured at different temperatures: 433, 413, 393, 363, 333, and 303 K. In all patterns, the filament axis had a vertical orientation with the X-ray beam perpendicular to the filament. The scattered intensity distributions were subsequently integrated along the equatorial and meridional axes, and the resulted intensities were plotted as a function of the scattering wave vector q (=$(4\pi/\lambda)$ sin $2\theta/2$, where θ is the scattering angle). Some representative images are shown in Figure 3.

The SAXS measurements were made using a 18 kW rotating-anode X-ray source with a pinhole collimation and a two-dimensional detector with 1024 × 1024 pixels. The sample-to-detector distance was set at 1.80 m. Measurements of 2 h long were made on cooling from 433 to 303 K.

Polarization Optical Microscopy (POM). A Zeiss microscope equipped with a Linkam THM600 hot stage was used for the investigation of the optical textures. All samples were cooled from 473 K at 2 K/min to 303 K, and the images were recorded with a CCD camera. Birefringent patterns were obtained at all temperatures exhibiting some singular points, as in bulk PBLG, usually found in nematic liquid crystals.

Differential Scanning Calorimetry (DSC). A Mettler Toledo Star DSC system was used with a heating/cooling rate of 10 K/min. A clear step in the specific heat ($\Delta c_P \approx 0.27$ J/(g K)) occurred only for the $PBLG_{50}$−$PDMS_{271}$−$PBLG_{50}$ copolymer at ∼297 K, corresponding to the PBLG glass transition temperature in the copolymer. Notice that this temperature is very close to the bulk PBLG T_g, suggesting phase separation. A lower T_g due to PDMS was not possible to extract from DSC.

Transmission and Scanning Electron Microscopy (TEM/STEM). For electron microscopy, bulk samples have been cryo-ultramicrotomed to a section thickness of approximately 60 nm. No additional staining of the samples was applied. TEM studies were performed on a LEO EM 912 with an Omega in-column spectrometer. The STEM studies were made on a FEI Tecnai F20 equipped with a high angular annular dark field (HAADF) detector using a diffraction length of 200 mm.

Dielectric Spectroscopy (DS). The sample cell consisted of two electrodes 20 mm in diameter and the sample with a thickness of 50 μm. The dielectric measurements were made at different temperatures in the range 113−413 K, at atmospheric pressure, and for frequencies in the range from 10^{-2} to 10^6 Hz using a Novocontrol BDS system composed of a frequency response analyzer (Solartron Schlumberger FRA 1260) and a broadband dielectric converter. The complex dielectric permittivity $\epsilon^* = \epsilon' - i\epsilon''$, where ϵ' is the real and ϵ'' is the imaginary part, is generally a function of frequency ω, temperature T, and pressure P, although here only the frequency and temperature dependences have been investigated. The analysis has been made using the empirical equation of Havriliak and Negami[35]

$$\frac{\epsilon^*(\omega, T) - \epsilon_\infty(T)}{\Delta\epsilon(T)} = \frac{1}{\{1 + [i\omega\tau_{HN}(T)]^\alpha\}^\gamma} \qquad (1)$$

where $\Delta\epsilon(T)$ is the relaxation strength of the process under investigation, τ_{HN} is the relaxation time of the equation, and α, γ ($0 < \alpha, \alpha\gamma \leq 1$) describe the symmetrical and asymmetrical broadening of the distribution of relaxation times. At lower frequencies, ϵ'' rises because of the conductivity ($\epsilon'' = \sigma/(\omega\epsilon_f)$, where σ is the dc conductivity and ϵ_f the permittivity of free space). The conductivity contribution has also been

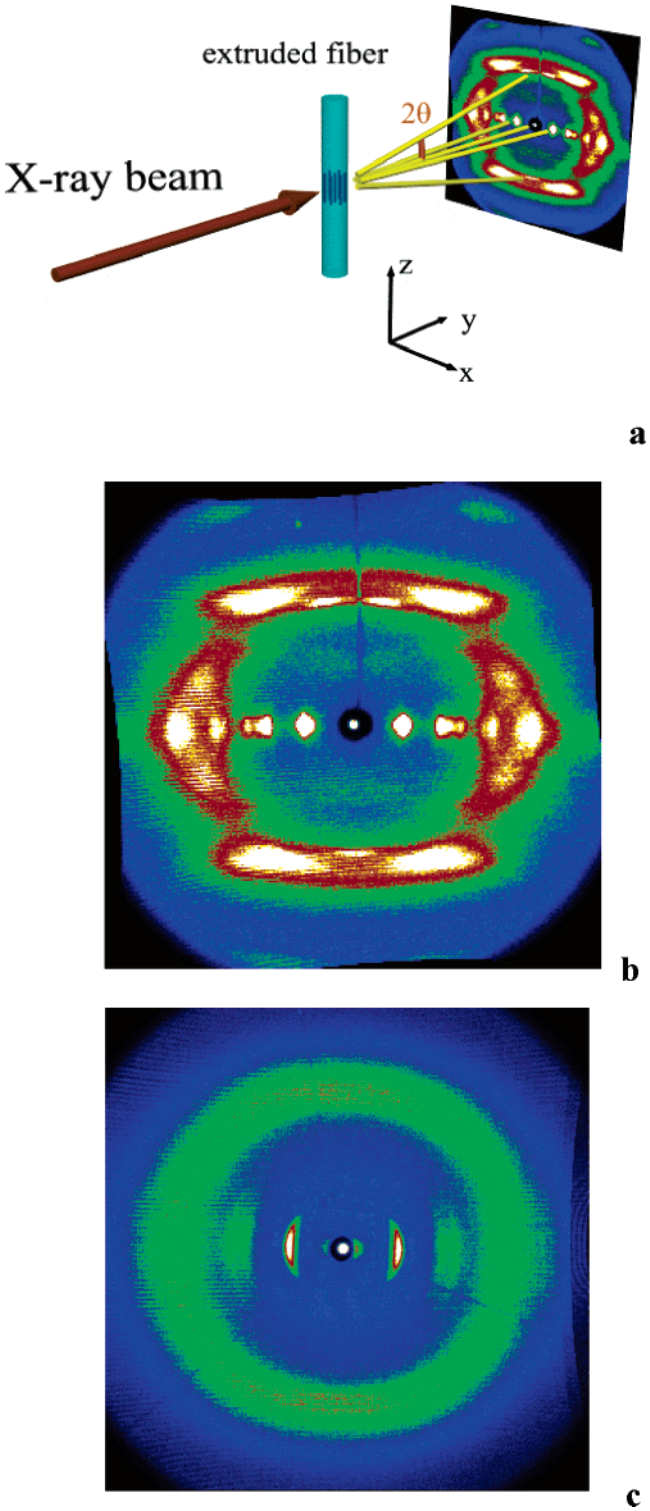

Figure 3. (a) Geometry of the 2D WAXS setup. The extruded fiber is placed normal to the X-ray beam and parallel to the 2D detector. (b) 2D WAXS image of a $PBLG_{42}$ fiber. The image is taken at 393 K, from an extruded fiber at 353 K following annealing at 393 K. The equatorial reflections suggest a hexagonal packing of the α-helices, whereas the α-helix pitch gives rise to the meridional reflections. (c) 2D WAXS image of a $PBLG_{50}$-*b*-$PDMS_{24}$-*b*-$PBLG_{50}$ fiber (T_{meas} = 413 K, T_{extr} = 373 K, T_{ann} = 413 K). The image comprises both reflections from the PBLG α-helices and the amorphous halo of PDMS. The higher-order equatorial reflections corresponding to PBLG can still be seen, despite being considerably weaker than in bulk PBLG. The PBLG α-helices in the copolymer are again hexagonally packed.

taken into account during the fitting process. The measured ϵ'' spectra have been used for the analysis except at high temperatures where the derivative of ϵ' has been employed ($d\epsilon'/d \ln \omega \approx -(2/\pi)\epsilon''$). Since ϵ' is not affected by the conductivity, this method is very useful in fitting relaxation processes which are hidden under the conductivity, provided that the system is free from polarization. The relaxation times at maximum loss (τ_{max}) have been analytically obtained by the Havriliak–Negami equation as follows

$$\tau_{max} = \tau_{HN}\left\{\frac{\sin\left[\frac{\pi\alpha}{2(1+\gamma)}\right]}{\sin\left[\frac{\pi\alpha\gamma}{2(1+\gamma)}\right]}\right\}^{-1/\alpha} \quad (2)$$

In addition to the dielectric permittivity, the electric modulus (M^*) representation was used.

$$M^* = \frac{1}{\epsilon^*} = M' + iM'' \quad (3)$$

The latter representation is very sensitive to the presence of slow processes as well as to the process due to ionic mobility. The ionic conductivity contribution can be observed as a maximum, where the M' and M'' curves cross. An asymmetric peak is an indication of a hidden relaxation process under the conductivity, as we will discuss in the following section. The relaxation times corresponding to maximum ϵ'' and M'' are related through $\tau_{M''} = \tau_{\epsilon''}(1 + \Delta\epsilon/\epsilon_\infty)^{-1/\alpha}$ in the case of symmetric distribution ($\gamma = 1$). Notice that for weak processes ($\Delta\epsilon \ll \epsilon_\infty$) the two representations give identical times.

III. Results and Discussion

Peptide Secondary Structure and Copolymer Phase State. Solid-state NMR is used both for the identification of the peptide secondary structure as well as for extracting some qualitative information on the copolymer phase state in comparison to the PDMS and PBLG homopolymer ^{13}C NMR spectra. The identification of the peptide secondary structure can be made from the distinctly different ^{13}C chemical shifts for the C_α and amide C═O resonances in the α-helical and β-sheet conformations.[36] For example, the C_α resonance at a chemical shift of $\delta \approx 58$ ppm is typical for PBLG α-helices as well as the amide C═O resonance at $\delta \approx 176$ ppm. In the β-sheet conformation, these chemical shifts are displayed upfield by about 4−5 ppm relative to the α-helical values. Since the amide C═O resonance in the β-sheet conformation partially overlaps with the signal from the side-chain ester, the distinction of the peptide secondary structure is best made from the distinctly different C_α resonances ($\delta \approx 58$ ppm and $\delta \approx 53$ ppm for α-helices and β-sheets, respectively).

The ^{13}C NMR spectra of Figure 2 reveal that the peptide secondary structure is predominantly α-helical when the degree of polymerization ($\langle x \rangle$) is 50 and 100, whereas β-sheets are formed when PBLG is very short ($\langle x \rangle = 5$), as anticipated from a previous study of PBLG polypeptides with variable degrees of polymerization.[7] Qualitative information on phase mixing in the copolymers can be obtained from the PDMS ^{13}C resonance at $\delta \approx 0$ ppm, which is assigned to the methyl carbons attached to the silicon atoms. In bulk PDMS (not shown here), as well as in the copolymers with the longer PBLG block (i.e., all the copolymers except of $PBLG_5$-*b*-$PDMS_{24}$-*b*-$PBLG_5$), such resonances at 0 ppm are absent (Figure 2), because pronounced local segmental mobilities (on the >100 kHz frequency scale) within the PDMS block prevents the spin polarization from being efficiently transferred between ^1H and ^{13}C. As such ^{13}C signal deficiencies are not observed for the PBLG blocks, it is evident that the PBLG adopts significantly different motional properties and, hence, needs to be phase-separated from the PDMS parts.

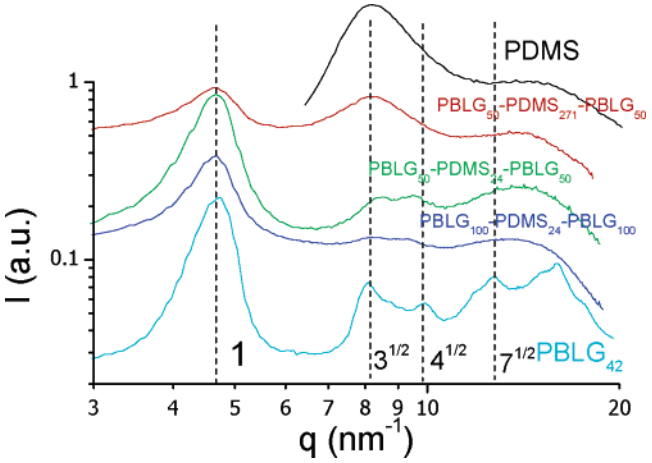

Figure 4. 2D WAXS equatorial intensities of a PDMS homopolymer (top), a PBLG homopolymer (bottom), and the three PBLG-*b*-PDMS-*b*-PBLG where the PBLG block was found to form helices. From top to bottom: (a) PDMS, (b) $PBLG_{50}-PDMS_{271}-PBLG_{50}$ (T_{meas} = 353 K, T_{extr} = 353 K, not annealed), (c) $PBLG_{50}-PDMS_{24}-PBLG_{50}$ (T_{meas} = 413 K, T_{extr} = 373 K, T_{ann} = 413 K), (d) $PBLG_{100}-PDMS_{24}-PBLG_{50}$ (T_{meas} = 413 K, T_{extr} = 353 K), and (e) $PBLG_{42}$ (T_{meas} = 393 K, T_{extr} = 353 K, T_{ann} = 393 K). The peaks designated as 1, $3^{1/2}$, and $4^{1/2}$ suggest a hexagonal packing of the PBLG helices.

In contrast to this, the ^{13}C spectrum of the $PBLG_5$-*b*-$PDMS_{24}$-*b*-$PBLG_5$ copolymer exhibits a strong dual resonance around $\delta \approx 0$ ppm, which means that the segmental mobility of the PDMS blocks is not as high anymore as in the other samples, but has become more similar to the dynamics of the PBLG parts. Moreover, the dual resonance implies two different environments for the two methyl carbons of the PDMS block, suggesting that a large number are adjacent to the PBLG monomers instead of siloxanes. The associated length scale is estimated at 0.5 nm, i.e., at a distance typical for the van der Waals proximity of atoms. These results reveal an intimate mixing between PDMS and PBLG segments in the $PBLG_5$-*b*-$PDMS_{24}$-*b*-$PBLG_5$ copolymer, while phase-separated structures exist in the other copolymers.

X-ray scattering was also employed for the determination of the peptide secondary structure in the copolymers. Two-dimensional wide-angle X-ray measurements were made using extruded and annealed fibers of the copolymers. A comparison between the $PBLG_{50}$-*b*-$PDMS_{24}$-*b*-$PBLG_{50}$ copolymer and a PBLG homopolymer is shown in Figure 3. PBLG displays a set of strong equatorial reflections with relative positions at $1:\sqrt{3}:\sqrt{4}:\sqrt{7}$ reflecting hexagonal packing of α-helices. As discussed earlier in detail, the WAXS pattern of bulk PBLG conforms to the paracrystalline form C; a nematic-like paracrystal with a periodic packing of α-helices in the direction lateral to the chain axis. For the copolymers with the long PBLG blocks, several broad equatorial reflections can be observed. Notice that reflections in the copolymers appear as arcs rather than sharp reflections, suggesting a distribution of orientations and a lower lateral coherence length. Nevertheless, their relative positions are $1:\sqrt{3}:\sqrt{4}$, revealing hexagonal packing of PBLG helices, similar to the respective homopolymer. The scattered intensities along the equator are compared in Figure 4. PDMS is liquid within the investigated temperature range and therefore gives rise only to two broad peaks at $q \approx 8$ nm^{-1}, known as the low van der Waals peak (LVDW), and $q \approx 15$ nm^{-1}, known as the van der Waals peak (VDW).[37] The position of the former peak overlaps with the higher-order peaks of the PBLG hexagonal lattice, and this is more evident in the copolymer with the higher PDMS content ($PBLG_{50}$-*b*-$PDMS_{271}$-*b*-$PBLG_{50}$, $f_{PBLG} = 0.57$). For the copolymer with the short PBLG block ($PBLG_5$-*b*-$PDMS_{24}$-*b*-$PBLG_5$), the WAXS pattern (not shown here) consists of the two main peaks of PDMS together with a shallow peak at $q \approx 3.5$ nm^{-1} originating from the PBLG β-sheet secondary structure.

The NMR (and WAXS) results suggest phase mixing for the $PBLG_5$-*b*-$PDMS_{24}$-*b*-$PBLG_5$ copolymer and phase-separated structures for the other copolymers. To obtain the nanodomain morphologies, we employed SAXS and TEM. The SAXS pattern from the $PBLG_{50}$-*b*-$PDMS_{24}$-*b*-$PBLG_{50}$ (f_{PBLG} 0.82) is depicted in Figure 5a at $T = 363$ K. It shows weak and broad peaks with approximate relative positions at 1:2, suggesting a lamellar nanodomain with a domain spacing of ~40 nm. A lamellar structure is also suggested by the TEM image in Figure 5b. Distinct dark areas separated by bright boundaries can be recognized in the figure. The dark areas are assumed to represent the PDMS-rich phase due to the Si content. Their average size was determined to be on the order of 30 nm, whereas the bright boundary areas have an average thickness of ~7 nm. Thus, the overall morphology can be described as cylinder-in-lamellar: PBLG cylinders within a lamellar nanodomain. This conclusion is not based on the current system that possesses very weak scattering contrast but to previous studies of rod-coil copolymers based on polypeptides. For example, for the PBLG-*b*-polyglycine diblock copolymer system, a stable lamellar nanodomain morphology was found for $f_{PBLG} = 0.79$.[21] Although theoretically predicted phase diagrams for peptidic block copolymers are still missing, the rodlike structure of one of the blocks is clearly responsible for the extended region of phase space with a flat interface.

Segmental Dynamics. Dielectric spectroscopy is a very sensitive probe of the local environment in polymer blends and copolymers and has been employed as a measure of phase mixing. In addition, DS allows the identification of the glass temperature for both blocks, which was a formidable task in DSC. We recall here that polypeptides exhibit a dynamic arrest at a temperature also known as the glass "transition"; this is an essential feature of protein dynamics that can inhibit biological function. The dynamic signature of this process is the strong nonexponentiality and the non-Arrhenius temperature dependence of relaxation times, $\tau(T)$. Despite its importance, the origin of this dynamic arrest was only recently clarified by studying the associated dynamics in different polypeptides as a function of molecular weight, temperature, pressure, and concentration, and as a function of the type of secondary structure (α-helical vs β-sheet)[6–8]. These studies revealed that the T_g is an intrinsic feature of polypeptide dynamics (i.e., not related to the solvent molecules) irrespective of the type of secondary structure originating from amorphous segments along the chain and at the chain-ends. Apart from this segmental (α-) process, different processes were found in the glassy state, with an Arrhenius *T*-dependence, originating from the side-chain dipoles as well as processes associated with the dynamics of the secondary structures at $T > T_g$ (to be discussed below). In addition to the polypeptide block, supercooled PDMS exhibits only a segmental (α-) process that becomes slower and weaker upon crystallization.[38]

The expectation born out from the DSC, NMR, and X-ray experiments for nanophase separation in all copolymers but the $PBLG_5$-*b*-$PDMS_{24}$-*b*-$PBLG_5$ copolymer should have direct consequences on the segmental dynamics for both blocks with processes indistinguishable from the respective homopolymers. In Figure 6, the imaginary part of the electric modulus (M'') is plotted as a function of frequency for the two homopolymers

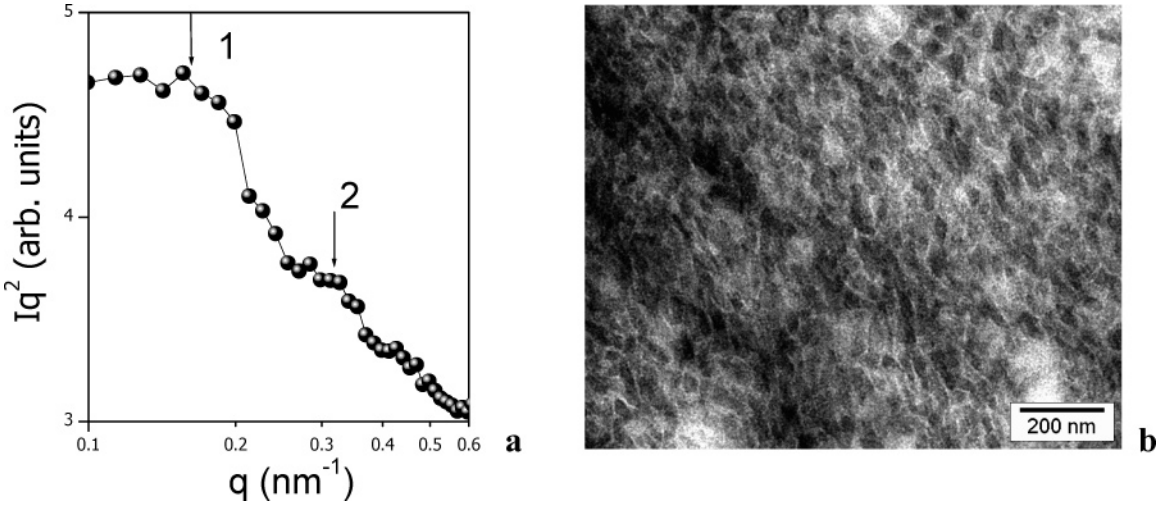

Figure 5. (a) Small-angle X-ray scattering from the $PBLG_{50}$-*b*-$PDMS_{24}$-*b*-$PBLG_{50}$ block copolymer ($f_{PBLG} = 0.93$) at $T = 363$ K. Two arrows are shown at relative position 1:2 with respect to the peak at $q \approx 0.16$ nm^{-1}, suggesting the formation of a lamellar microdomain morphology. The reflections are very weak because of the low contrast. (b) TEM bright field (BF) micrograph of the same sample.

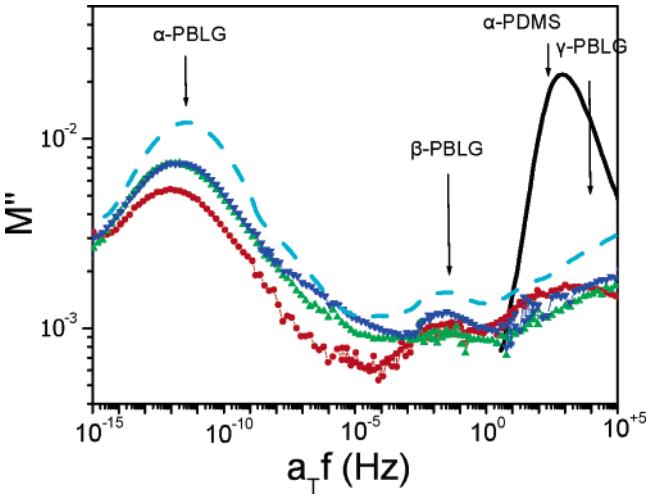

Figure 6. Superposition of the imaginary part of the electric modulus (M'') for the PDMS (solid line) and PBLG (dashed line) homopolymers and three copolymers; $PBLG_{50}$-*b*-$PDMS_{271}$-*b*-$PBLG_{50}$ (circles); $PBLG_{50}$-*b*-$PDMS_{24}$-*b*-$PBLG_{50}$ (up triangles); $PBLG_{100}$-*b*-$PDMS_{24}$-*b*-$PBLG_{100}$ (down triangles). The reference temperature is $T = 153$ K. The copolymer with the higher PDMS content (50-271-50, $f_{PDMS} = 0.57$) exhibits relaxation maxima at locations corresponding exactly to the respective homopolymers; the other two copolymers exhibit all the processes corresponding to the PBLG blocks, but the high intensity of the PBLG γ-process precludes the resolution of the PDMS segmental process.

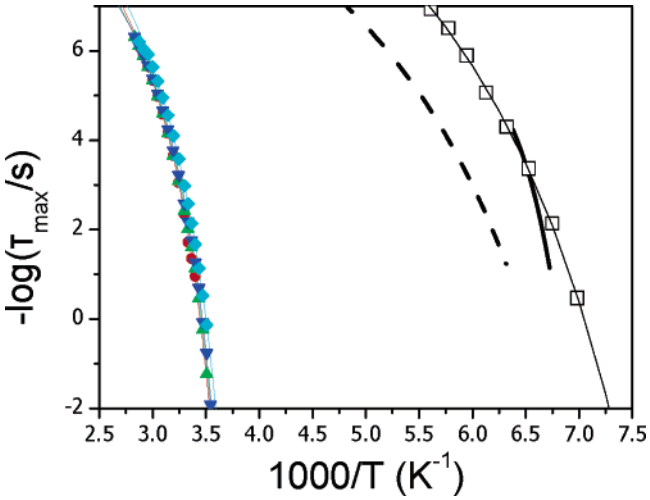

Figure 7. Arrhenius plot of the segmental relaxation times at maximum loss (and M'') of the samples shown in Figure 6. The secondary (β-), intermediate, and "slow" processes are omitted for clarity: PDMS segmental (α-) process in the $PBLG_{50}$-*b*-$PDMS_{271}$-*b*-$PBLG_{50}$ copolymer (open symbols); PBLG segmental (α-) process in the different copolymers (filled symbols); $PBLG_{50}$-*b*-$PDMS_{271}$-*b*-$PBLG_{50}$ (circles); $PBLG_{50}$-*b*-$PDMS_{24}$-*b*-$PBLG_{50}$ (up triangles); $PBLG_{100}$-*b*-$PDMS_{24}$-*b*-$PBLG_{100}$ (down triangles); $PBLG_{42}$ homopolymer (rhombus). The continuous and dashed lines correspond to the times for amorphous and semicrystalline PDMS, respectively.[38]

and three copolymers. The extended frequency range is obtained by applying, at each temperature, a single frequency-scale shift factor a_T that allows the superposition of the data at temperature T with the data at the reference temperature ($T_{ref} = 153$ K). The superposition is made with respect to the PBLG segmental relaxation in the copolymers and is only approximately valid, since the different processes involved display different T-dependencies. Nevertheless, the different processes can be compared in this approximation, but for obtaining the exact τ-(T), we have used the fitting procedure to each (unshifted) curve as explained in the experimental part. In Figure 6, the PBLG segmental process can be clearly observed in all copolymers, despite its lower amplitude, with a rate indistinguishable from the corresponding process in bulk PBLG in agreement with the single T_g from DSC. Similarly, the PDMS segmental process in the $PBLG_{50}$-*b*-$PDMS_{271}$-*b*-$PBLG_{50}$ ($f_{PBLG} = 0.57$) copolymer, i.e., the copolymer with the highest PDMS content, is relaxing with the same rate as bulk PDMS. The reduced intensity of the PDMS α-process in the copolymer is due to the crystallization of PDMS at 153 K. This is supported by a DSC trace showing a step at ~290 K (i.e., the PBLG T_g) and an endothermic peak at ~233 K, corresponding to the fusion of PDMS crystals. Notice that for the copolymers with the lower PDMS content the high intensity of the PBLG γ-process precludes the resolution of the PDMS segmental process. Nevertheless, the location of the segmental (α-) process corresponding to the PBLG block and of the PDMS segmental process in the $PBLG_{50}$-*b*-$PDMS_{271}$-*b*-$PBLG_{50}$ copolymer provide a clear signature of nanophase separation in agreement with the X-ray and NMR results.

The segmental relaxation times, corresponding to the M''_{max}, for both blocks and the corresponding homopolymers are plotted in Figure 7 in the usual Arrhenius representation. In the same figure, we include α-relaxation times of amorphous and sem-

icrystalline PDMS, for comparison. All $\tau(T)$ conform to the Vogel−Fulcher−Tammann equation

$$\tau = \tau_0 \exp \frac{D_T T_0}{T - T_0} \quad (4)$$

where τ_0 is the "primitive" relaxation time corresponding to very high T, D_T is a dimensionless parameter, and T_0 is the "ideal" glass temperature. For the PBLG segmental process in the copolymers, these parameters are $\tau_0 \approx 4.0 \times 10^{-12}$ s, $D_T = 5.4$, and $T_0 = 241$ K, whereas for the PDMS segmental process in the PBLG$_{50}$-*b*-PDMS$_{271}$-*b*-PBLG$_{50}$ copolymer, they are $\tau_0 \approx 1.6 \times 10^{-14}$ s, $D_T = 10.6$, and $T_0 = 106.2$ K. Again, these parameters are very close to the corresponding parameters in the homopolymers (τ_0, D_T, and T_0 assume values of 2.5×10^{-12} s, 5.8, 235 K, respectively, for PBLG and 1.6×10^{-14} s, 5.9, and 123 K for PDMS, respectively), revealing nanophase-separated structures.

Dynamics of the Secondary Structure. The dynamics of the secondary structure (α-helix) can be obtained from DS from the slower and more intense process associated, in principle, with the end-to-end relaxation of dipoles in a perfect α-helical structure. DS is very sensitive not only to the presence of α-helices, but also to their persistence length. In this respect, we have recently shown that, contrary to the expectation born out by the static experiments and common belief, α-helical polypeptides cannot be considered as ideal rigid rods and that a model of "broken" rods is closer to reality. This is based on the fact that there exist two processes above the T_g that are slower than the segmental (α-) process: an "intermediate" process which has strong molecular weight dependence and reflects the relaxation of amorphous parts of PBLG chains, and a "slow" process which reflects the relaxation of α-helical defects. The persistence length ξ of the α-helical structure can be extracted from the intensity of the slower DS process. In a study of PBLG as a function of molecular weight, ξ was found in the range 1−2 nm, i.e., comprising about 10−20 monomers.[7,8]

In view of recent results, it would be of interest to explore the effect of the intermediate flexible polymer (PDMS) on the persistence length of PBLG α-helices. A first indication for increasing persistence length is the slowing-down of the PBLG "slow" process, which, as we explained above, is attributed to the relaxation of helical defects. This is depicted in Figure 8, where the real and imaginary parts of M^* for the PBLG$_{50}$-*b*-PDMS$_{271}$-*b*-PBLG$_{50}$ copolymer are compared with respect to the PBLG homopolymer. The peak of M'' curve near the crossing point of M' and M'' is mainly due to the conductivity, but its asymmetric shape at higher frequencies implies the existence of the "slow" process. Notice that this peak in the block copolymer is shifted to longer times by about one decade, indicating the slowing-down of the relaxation times associated with the slower process. In addition, it is more asymmetric because of the enhanced intensity of the "slow" process. Both trends are a strong indication that the α-helical persistence length of PBLG increases in the presence of PDMS despite the lower lateral coherence of helices as revealed by WAXS. To make the comparison more quantitative, we plot in Figure 9 the effective dipole moment corresponding to the "slow" process for the three copolymers. The dipole moment was calculated using two different methods: The first is the Fröhlich equation, which is more suitable for spherical molecules

$$\Delta\epsilon = \frac{NgF\mu^2}{3\epsilon_0 k_B T} \quad (5)$$

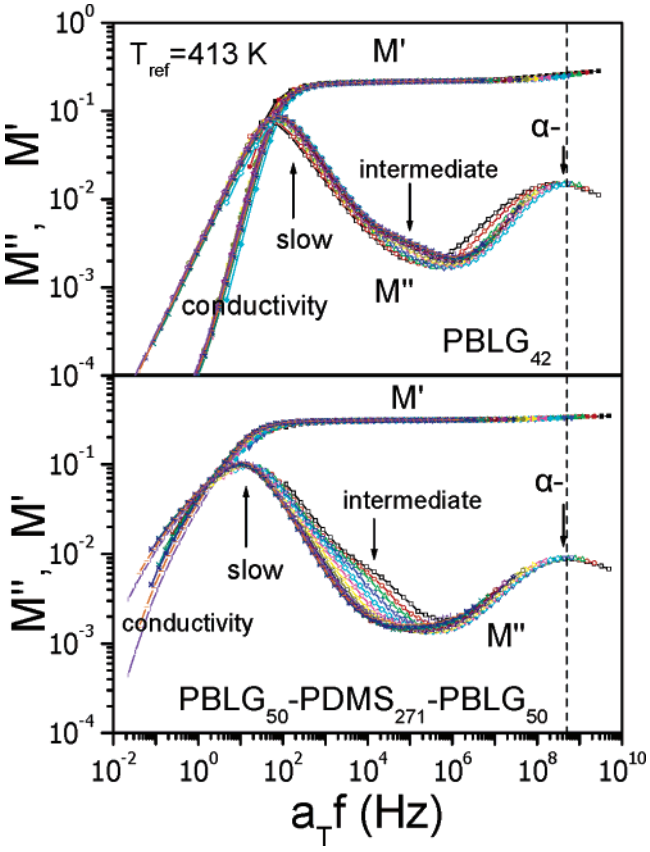

Figure 8. Superpositions of the real (M', filled symbols) and imaginary (M'', open symbols) parts of the electric modulus M^* of a PBLG$_{42}$ homopolymer (top) and the PBLG$_{50}$-*b*-PDMS$_{271}$-*b*-PBLG$_{50}$ copolymer ($f_{PBLG} = 0.57$) (bottom). The reference temperature is $T = 413$ K. The crossing of the M' and M'' curves at low frequencies is due to the ionic conductivity. Notice the asymmetry of the M'' curve around the maximum, which is caused by a slower process in the proximity of the ionic conductivity that is attributed to the motion of defects along the α-helix.

where μ is the dipole moment, N is the number density of dipoles, $g = 1 + \langle \cos \gamma \rangle$ is the Kirkwood−Fröhlich correlation factor between neighboring dipoles and $F = [(\epsilon_\infty + 2)/3]^2[3\epsilon_s/(2\epsilon_s + \epsilon_\infty)]$ is the local field correction factor, where ϵ_s and ϵ_∞ are the permittivity values at the low- and high-frequency limit, respectively. The second is the Buckingham equation[39] (modified by Applequist and Mahr[24])

$$\frac{Nfg\mu^2}{3\epsilon_0 k_B T} = \frac{(2\epsilon_s + 1)(\epsilon_s - n^2)}{2\epsilon_s + n^2} - \frac{(2\epsilon_\infty + 1)(\epsilon_\infty - n^2)}{2\epsilon_\infty + n^2} \quad (6)$$

where f is a value related to the geometry of the molecule ($f \rightarrow {}^2/_3$ for an infinitely long rod) and n is the refractive index. This equation describes better rodlike molecules in solutions and is probably more suitable in the present case. The dashed line shows the respective values for a series of PBLG homopolymers, and the solid line is the theoretical value for an ideal α-helix. The effective dipole moments of the two block copolymers with high PBLG content (PBLG$_{50}$-*b*-PDMS$_{24}$-*b*-PBLG$_{50}$ and PBLG$_{100}$-*b*-PDMS$_{24}$-*b*-PBLG$_{100}$) show almost no difference from the PBLG homopolymer with the same molecular weight. The PBLG$_{50}$-*b*-PDMS$_{271}$-*b*-PBLG$_{50}$ case with the higher PDMS content, however, is different; the dipole moment is much higher than the homopolymer (by about a factor of 2) although still lower than the theoretical value.

Understanding this effect requires some knowledge of the block copolymer phase state.[40] Block copolymer segregation is

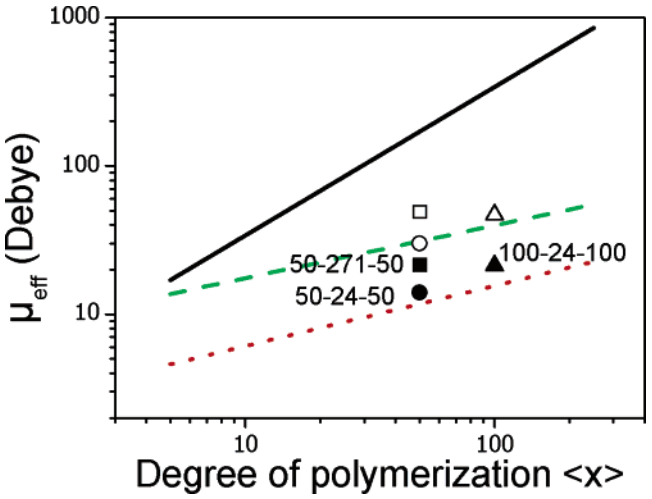

Figure 9. Effective dipole moments of the $PBLG_{50}-PDMS_{271}-PBLG_{50}$ (f_{PBLG} = 0.57, squares), $PBLG_{50}-PDMS_{24}-PBLG_{50}$ (f_{PBLG} = 0.93, circles), and $PBLG_{100}-PDMS_{24}-PBLG_{100}$ (f_{PBLG} = 0.96, triangles) copolymers corresponding to the slower process. Solid symbols correspond to the effective dipole moments calculated using the Fröhlich equation, whereas the values obtained from the Buckingham equation are depicted with hollow symbols. The continuous line is the theoretical dipole moment for an ideal α-helix (3.4 D per monomer[25]), whereas the dashed and dotted lines show the dipole moments obtained for a series of PBLG homopolymers,[7] calculated using the Fröhlich and Buckingham methods, respectively.

influenced by (i) the segment−segment interaction parameter χ, describing the free energy cost per monomer of contacts between unlike monomers and (ii) the total degree of polymerization N, affecting the translational and configurational entropy of chains. Since the entropic and enthalpic contributions to the free energy scale as N^{-1} and χ, respectively, the phase state of block copolymers is discussed in terms of the product χN. Other effects, such as the conformational asymmetry, copolymer architecture, and fluctuation effects, can strongly influence the phase state and have been discussed in detail in the literature. For strongly segregated copolymers (i.e., $\chi N \rightarrow \infty$), chains are strongly stretched and can be envisioned as grafted polymer brushes with a domain period scaling as $d \approx N^{2/3}\chi^{1/6}$, i.e., with a strong N-dependence. Following these ideas, the thermodynamic confinement and chain stretching should be more pronounced in the $PBLG_{50}$-*b*-$PDMS_{271}$-*b*-$PBLG_{50}$ copolymer as compared to the $PBLG_{50}$-*b*-$PDMS_{24}$-*b*-$PBLG_{50}$ because of the higher N and possibly by the more symmetric composition (the latter statement assumes symmetric phase behavior) that drives the copolymer deeper into the phase-segregated region. This chain stretching gives rise to the partial annihilation of helical defects and the more persistent helical sequences as observed experimentally. We mention here that a similar effect was observed in the PBLG-*b*-PGly diblock copolymers as well as in the PBLG-*b*-PEO-*b*-PBLG triblock copolymer system. This suggests that thermodynamic confinement can be employed as a means of secondary structure perfection in phase-separated polypeptide block copolymers.

IV. Conclusions

A series of PBLG-*b*-PDMS-*b*-PBLG triblock copolymers were studied using ^{13}C NMR, SAXS/WAXS, and TEM for the investigation of the structure and dielectric spectroscopy (DS) for the dynamics, respectively. The main results of the present study are as follows:

1. Phase segregation occurs in the copolymers with the longer peptide blocks, resulting in PBLG α-helical segments embedded within the block copolymer nanodomains.

2. The lateral coherence length of the PBLG hexagonal lattice composed of α-helices decreases as compared to bulk PBLG due to the PDMS block.

3. Dielectric spectroscopy revealed that the PBLG α-helices are not perfect, i.e., they contain amorphous "defects" as in the PBLG homopolymers.

4. However, the persistence length of the α-helical structures was found to depend on the copolymer number of segments N and composition f. This effect is discussed in terms of the strong segregation and the thermodynamic confinement of the segments within the nanodomains giving rise to the partial annihilation of helical defects. Thus, increasing thermodynamic confinement and the associated chain stretching can be employed as a means of increasing the "perfection" of α-helices.

Acknowledgment. This work was funded by a GSRT grant (PENED529).

References and Notes

(1) Muthukumar, M.; Ober, C. K.; Thomas, E. L. *Science* **1997**, *277*, 1225.
(2) Walton, A. G.; Blackwell, J. In *Biopolymers*; Academic Press: New York, 1973.
(3) Harrison, P. M.; Bamborough, P.; Duggett, V.; Prusiner, S. B.; Cohen, F. E. *Curr. Opin. Struct. Biol.* **1997**, *7*, 53.
(4) Doster, W.; Cusack, S.; Petry, W. *Nature (London)* **1989**, *337*, 754.
(5) Iben, I. E. T.; Braunstein, D.; Doster, W.; Frauenfelder, H.; Hong, M. K.; Johnson, J. B.; Luck, S.; Ormos, P.; Schulte, A.; Steinbach, P. J.; Xie, A. H.; Young, R. D. *Phys. Rev. Lett.* **1989**, *62*, 1916.
(6) Papadopoulos, P.; Floudas, G.; Schnell, I.; Klok, H.-A., Aliferis, T.; Iatrou, H.; Hadjichristidis, N. *J. Chem. Phys.* **2005**, *122*, 224906.
(7) Papadopoulos, P.; Floudas, G.; Klok, H.-A.; Schnell, I.; Pakula, T. *Biomacromolecules* **2004**, *5*, 81.
(8) Papadopoulos, P.; Floudas, G. *Dielectric Newsletter*, October 2005.
(9) Aliferis, T.; Iatrou, H.; Hadjichristidis, N. *Biomacromolecules* **2004**, *5*, 1653.
(10) Lecommandoux, S.; Achard, M.-F.; Langenwalter, J. F.; Klok, H.-A. *Macromolecules* **2001**, *34*, 9100.
(11) Douy, A.; Gallot, B. *Polymer* **1982**, *23*, 1039.
(12) Klok, H.-A.; Langenwalter, J. F.; Lecommandoux, S. *Macromolecules* **2000**, *33*, 7819.
(13) Babin, J.; Rodriguez-Hernandez, J.; Lecommandoux, S.; Klok, H.-A.; Achard, M.-F. *Faraday Discuss.* **2004**, *218*, 1.
(14) Schlaad, H.; Antonietti, M. *Eur. Phys. J. E* **2003**, *10*, 17.
(15) Schlaad, H.; Smarsly, B.; Losik, M. *Macromolecules* **2004**, *37*, 2210.
(16) Schlaad, H.; Kukula, H.; Smarsly, B.; Antonietti, M.; Pakula T. *Polymer* **2002**, *43*, 5321.
(17) Minich, E. A.; Nowak, A. P.; Deming, T. J.; Pochana, D. J. *Polymer***2004**, *45*, 1951.
(18) Floudas, G.; Papadopoulos, P.; Klok, H.-A.; Vandermeulen, G. W. M.; Rodriguez-Hernandez, J. *Macromolecules* **2003**, *36*, 3673.
(19) Wu, G. L.; Sun, P. C.; Lin, H.; Ma, J. B *J. Mol. Struct.* **2004**, *689*, 143.
(20) Kim, H. J.; Choi, E. Y.; Oh, J. S.; Lee, H. C.; Park, S. S.; Cho C. S. *Biomaterials* **2000**, *21*, 131.
(21) Papadopoulos, P.; Floudas, G.; Schnell, I.; Aliferis, T.; Iatrou, H.; Hadjichristidis, N. *Biomacromolecules* **2005**, *6*, 2352.
(22) Erenrich, E. H.; Scheraga, H. A. *Macromolecules* **1972**, *5*, 746.
(23) Matsumoto, T.; Nishioka, N.; Teramoto, A.; Fujita, H. *Macromolecules* **1974**, *7*, 824.
(24) Applequist, J.; Mahr, T. G. *J. Am. Chem. Soc.* **1966**, *88*, 5419.
(25) Wada, A. *J. Chem. Phys.* **1958**, *29*, 674; **1959**, *30*, 328; **1959**, *30*, 324.
(26) Mori, Y.; Ookubo, N.; Hayakawa, R.; Wada, Y. *J. Polym. Sci.: Polym. Phys. Ed.* **1982**, *20*, 211.
(27) Moscicki, J. K.; Williams, G. *J. Polym. Sci.: Polym. Phys. Ed.* **1983**, *21*, 197; **1983**, *21*, 213.
(28) Romero Colomer, F. J.; Gomez Ribelles, J. L.; Barrales-Rienda, J. M. *Macromolecules* **1994**, *27*, 5004.
(29) Romero Colomer, F.; Gomes Ribelles, J. L.; Lloveros Macia, J.; Guerra Munoz, S. *Polymer* **1991**, *32*, 1642.

(30) Watanabe, J.; Uematsu, I. *Polymer* **1984**, *25*, 1711.
(31) Schmidt, A.; Lehmann, S.; Georgelin, M.; Katana, G.; Mathauer, K.; Kremer, F.; Schmidt-Rohr, K.; Boeffel, C.; Wegner, G.; Knoll, W. *Macromolecules* **1995**, *28*, 5487.
(32) Hartmann, L.; Kratzmuller, T.; Braun, H.-G.; Kremer, F. *Macromol. Rapid Commun.* **2000**, *21*, 814.
(33) Kania, C. M.; Nabizadeh, H.; McPhillimy, D. G.; Patsiga, R. A. *J. Appl. Polym. Sci.* **1982**, *27*, 139.
(34) Kumaki, T.; Sisido, M.; Imanishi, Y. *J. Biomed. Mater. Res.* **1985**, *19*, 785.
(35) Havriliak, S.; Negami, S. *Polymer* **1967**, *8*, 161.
(36) Shoji, A.; Ozaki, T.; Saito, H.; Tabeta, R.; Ando, I. *Macromolecules* **1984**, *17*, 1472.
(37) Arrighi, V.; Higgins J. S.; Burgess, A. N.; Floudas, G. *Polymer* **1998**, *39*, 6369.
(38) Kirst, K. U.; Kremer, F.; Litvinov, V. M. *Macromolecules* **1993**, *26*, 975.
(39) Buckingham, A. D. *Aust. J. Chem.* **1953**, *6*, 93, 323.
(40) Hadjichristidis, N.; Pispas, S.; Floudas, G. In *Block Copolymers: Synthetic Strategies, Physical Properties and Applications*; J. Wiley & Sons: Hoboken, NJ, 2003.

BM050772T